Deep geothermal energy in northern England: insights from 3D finite difference temperature modelling

Louis Howell[1]*, Christopher S. Brown[2], Stuart S. Egan[1]

Authorship statement

- Louis Howell: compiled metadata, constructed model, wrote manuscript
- Christopher Brown: helped construct model and write manuscript
- Stuart Egan: helped construct model and write manuscript

Code availability

Source code is available via https://github.com/lphowell/Geothermal-Modelling/tree/master/Geothermal_NEngland or by contacting the lead author.

Highlights

- Subsurface temperature and heat flow maps for northern England are produced by temperature modelling
- These maps are more resolute and geologically more realistic relative to equivalent contoured maps for the UK
- Temperature models highlight ‘hot spots’ associated with granite intrusions and geological structure
- This technique comprises a potentially useful tool for deep geothermal energy exploration

Key words

Geothermal Energy; Temperature; Finite Difference; Numerical Modelling

Abstract

Many of the most widely used deep geothermal resource maps for the UK are produced by contouring around sparsely distributed and often unreliable data points. We thus present a MATLAB-based 3D finite difference temperature modelling methodology, which provides a means for producing more resolute and geologically realistic versions of these maps. Our case study area in northern England represents an area where both sedimentary basins and radiothermal granite bodies comprise potential geothermal resources. We divide our 3D model into geological units, which are then assigned separate thermal properties. Assuming conductive heat transfer and steady-state and fixed boundary conditions, we calculate 3D regional subsurface temperature. Due to our averaging technique for thermal properties, the resolution of our geological model is scarcely compromised with respect to similar finite element methods. One predicted ‘hot spot’ at 1 km depth in the central part of our case study area corresponds with the granitic North Pennine Batholith. Other shallow hot spots correspond with thermally insulating sedimentary rock units and geological structures that incorporate these units. Predictive heat flow density maps highlight areas with accelerated surface heat flow associated with shallow conductive basement rock and heat producing granite bodies. Our predicted subsurface temperatures show broad similarities with measured

equilibrium borehole temperatures. Inaccuracies may relate to convective heat transfer involving fault systems, or input variables relating to the geological model. Our predictive subsurface temperature and heat flow density maps are more resolute and geologically realistic relative to pre-existing contoured maps. The method presented here represents a useful tool for understanding controls on subsurface temperature distribution and geothermal potential.

1. Introduction

Geothermal may provide one alternative energy resource as part of a worldwide effort to reduce our reliance on fossil fuels and combat climate change (Zhang *et al*., 2019). Nonetheless, the UK lags its neighboring north-western European counterparts with regards to harnessing its deep geothermal potential. This is reflected by the fewer number of geothermal boreholes drilled (Gluyas *et al*., 2018), the smaller contribution of geothermal towards the combined energy mix (BP Energy Outlook, 2019), smaller research output, and the now somewhat outdated subsurface temperature and heat flow maps for the UK (e.g. Downing and Gray, 1986a, 1986b; Lee *et al*., 1987; Busby, 2010, 2014; Busby *et al*. 2011). These maps are commonly constructed by contouring around sparsely distributed and sometimes unreliable data points (Rollin, 1995), rendering them often irresolute and inaccurate (Fig. 1). Despite increasing interest in UK geothermal, as several recent and ongoing projects testify to (Younger *et al*., 2016; Adams *et al*., 2019; Monaghan *et al*., 2019; Paulillo *et al*., 2020), the reliance on these quasi-resource maps remains a cause for concern.

Where data is either sparse or unreliable, predictive modelling may comprise a useful tool (Pérez-Zárate *et al*., 2019). Numerically based 3D regional subsurface temperature models help communicate regional geothermal potential (e.g. Cacace *et al*., 2010; Calcagno *et al*., 2014; Fuchs and Balling, 2016). Such models typically implement elaborate, but often complex and, consequently, less reproducible finite element techniques (e.g. Cacace and Jacquey, 2017). Finite difference analyses offer less computationally intensive alternatives to these methods. Although the resolution and accuracy of finite difference models are limited by the typically rectangular nodal arrangements of finite difference grids, for smaller problems, such as for the (<1 km) area around a geothermal well head, a finite difference grid can be sufficiently scaled to compromise between both model accuracy and rapid model convergence (e.g. Croucher *et al*., 2020; Keller *et al*., 2020). Finite difference techniques are also adopted for subsurface temperature problems where the geological uncertainty is greater than the model resolution, such as for the deep lithosphere and mantle (e.g. Fullea *et al*., 2009). However, for intermediate scale problems, such as for subsurface temperature and heat flow density mapping (e.g. Fig. 1), a combination of the often inflexible finite difference temperature grids, and the coarse model resolutions required to reduce run times, can render such methods too inaccurate (*cf*. Gibson *et al*., 2008).

We present an innovative 3D finite difference thermal modelling method that is used to predict deep subsurface temperature and heat flow density in northern England. Due to our averaging techniques for thermal conductivity and radiogenic heat production values, the resolution of our geological model is effectively far greater than the temperature model's coarse nodal spacing. Consequently, the accuracy of our model is not compromised to reduce computational intensity. We document formulae and include MATLAB script with supplementary information for 3D steady-state conductive heat transfer. Comparisons are made between results from our simulations and measured borehole temperatures and heat flow densities. This technique represents some key influences of complex geological structure on subsurface temperature distribution. Its main strengths are its robustness, simplicity and reproducibility relative to more elaborate finite element techniques. Compared to other finite difference techniques, our methodology offers more resolute and geologically more realistic solutions. We present and discuss the UK's first deep 3D temperature model and associated geothermal resource maps.

2. Study area: northern England

Our case study area comprises an area of the UK where both sedimentary basins and ancient granite bodies comprise potential geothermal resources (Gluyas *et al*., 2018). Together, it comprises the northern part of the Lake District, the north-east of England and the Scottish borders (Fig. 2). The primary energy demand for this region is roughly along the north-east coast and includes Newcastle-upon-Tyne and Sunderland. Besides Carlisle, the remainder of our study area is amongst the most sparsely populated areas of England. Ideally for the purposes of our study, this is an area that has had widely documented but ultimately unsuccessful geothermal exploration (Gluyas *et al*., 2018).

Despite the magnitude of recent investments in geothermal exploration in northern England (Manning *et al*., 2007; Hirst, 2012; Younger *et al*., 2016), what we know about deep subsurface temperatures and heat flow in the region is based upon somewhat outdated quasi-resource maps (e.g. Downing and Gray, 1986a; Busby *et al*., 2011) (Fig. 1). In our study area, for example, maps depicting temperature at 1 km depth are based on contours around just six temperature data points (Fig. 3). These data are situated predominantly within the Carboniferous basins of the region and only two of these are equilibrium measurements (Burley *et al*., 1984). On further inspection of these maps and the UK Geothermal Catalogue (Burley *et al*., 1984), heat flow density maps for this region are based on contours around just 9 data points (Fig. 1b). Based on the type of conductivity and temperature measurement, amongst other factors, Rollin (1995) graded the reliability of these data with quality functions from 0 to 1, with 1 being good and 0 being poor. The highest grade awarded for a data point in our study area was 0.65. Just five data points surpassed 0.25.

3. Data

A 3D subsurface geological model of northern England comprises the primary dataset of our study (Fig. 4). A structural model of the Carboniferous-Permian basins of our study area is based on the seismic interpretations of Chadwick *et al*. (1995) (*cf*. Terrington and Thorpe, 2013). The structure of pre-Carboniferous basement bound Caledonian granites are based upon the gravity interpretations of Kimbell *et al*. (2010). The bases of these granite intrusions are assumed flat at 9 km depth (*cf*. Kimbell *et al*., 2010) (Fig. 4). Our geological model does not include the Cheviot granites or other granites along the Southern Uplands, which are located beyond the northern margin of our study area. Our model's geological boundaries are derived from several 2D nodal grids of elevation values based on these metadata. The boundaries that are derived from these data are extrapolated to fill a 110 km by 150 km grid. The coordinates at which elevation values are given each correspond to separate nodes within our temperature grid and are uniformly spaced.

The geological boundaries within our model separate geological units, which are assigned distinct thermal properties (Table 1). Thermal conductivity of the crust is a function of temperature and pressure, as well as composition (Norden *et al*., 2020); therefore, conductivity of middle-lower crustal rock decreases with depth (and temperature). Thermal properties for basement rock and basin fill are based on numerous literary sources (e.g. Čermác and Rybach, 1982; Downing and Gray, 1986; Norden and Förster, 2006; Manning *et al*., 2007; Norden *et al*., 2008; Vilá *et al*., 2010; Younger *et al*., 2016; Busby, 2019). Borehole temperatures for comparison with our modelled subsurface temperature grid are derived from the UK Geothermal Catalogue (Burley *et al*., 1984) and published literature (e.g. Younger *et al*., 2016). Typically, finite difference techniques dictate that the thermal property matrices within temperature models are divided into a series of variably sized cuboids, the volume of which are defined by the temperature grids nodal spacing (e.g. Fullea *et al*., 2009). However, in Section 4.3 we detail how more geologically realistic thermal property matrices may be derived from a geological model, whilst still implementing a less computationally intensive finite difference methodology and coarse nodal spacing.

4. Methods

A summary of our modelling approach is illustrated in Figure 5. These methods may be amended depending on the characteristics of geological models or the specifications of subsurface temperature models, although the crux of this technique may remain unchanged. We recommend that the meshing process is treated separately from temperature simulation, to reduce memory drainage and ultimately reduce temperature convergence times.

4.1 Governing equations

To calculate subsurface temperature, we solve a steady-state conductive heat equation, or diffusion equation according to Fourier's law. The diffusion equation operates on the basis of energy conservation and relates heat flow (q) to temperature gradients (∇T). In its differential form, it can be given as:

$$q = -k \, \nabla T$$

(Eq. 1)

where k is the bulk rock thermal conductivity tensor. Temperature change experienced by each node within the temperature grid is equal to the heat conducted into or out of a node, plus radiogenic heat production (Q). Thus the following relationship between change in heat flow (∇q) and time (t) can be determined:

$$(\rho \ c)\frac{\partial T}{\partial t} = -\nabla q + Q$$

(Eq. 2)

where ρ is the bulk rock density and c is the bulk specific heat capacity. When Equation 1 is substituted into Equation 2, the equation for transient diffusion is given:

$$(\rho \ c)\frac{\partial T}{\partial t} = \nabla(k \, \nabla T) + Q$$

(Eq. 3)

Under steady-state conditions, any transient effect is neglected. Therefore, the equation can be rearranged further as thus:

$$\nabla(k \, \nabla T) = -Q$$

(Eq. 4)

This equation is solved for the temperature using a 3D implementation of the finite difference methodology with algorithms developed using the MATLAB (Mathworks) numerical computing environment.

4.2 Boundary conditions and model validation

The solution to Equation 4 using the finite difference method requires definition of boundary conditions. For subsurface thermal modelling, we adopt an upper boundary (surface) temperature of 10 °C, in concurrence with UK annual mean average air temperature (Busby *et al.*, 2009). The lower boundary temperature at the base of our model represents a more irreconcilable problem. The base of the lithosphere is at a depth of approximately 125 km beneath much of north-western Europe and is represented by the 1333 °C isotherm (Sclater and Christie, 1980).

To validate the differential solution against an analytical solution in one-dimension and determine the likely lithosphere-scale geothermal structure of our case study area, we reiterate the linear equation until an asymptotic solution, our modelled geothermal gradient, is reached (Fig. 6). When adopting a uniform grid spacing of 1 km, the modelled geothermal gradient approaches its steady state solution after approximately 10,000 iterations. To reduce convergence time, the temperature matrix can be populated with a pre-defined temperature distribution (e.g. Bayer *et al.*, 1997) or be thermally conditioned using temperatures from previous model simulations. Besides boundary temperatures, thermal conductivity has a primary control on the geothermal gradient. The decreased geothermal gradient with depth, after 30 km, reflects the increased thermal conductivity of mantle rock relative to crustal rock below the Moho boundary (e.g. Čermác and Rybach, 1982) (Table 1). With the addition of radiogenic heat production, the modelled geothermal gradient forms a convex upwards curve.

The lateral boundaries of our 3D model, in the x and y directions, are closed. Thus $\delta T/\delta x$ = 0, and $\delta T/\delta y$ = 0. This implies no heat is transferred beyond the lateral boundaries of the model and that these boundaries represent surfaces of symmetry. Neither of these assumptions fit reality but they provide approximations for complex geological structures. To reduce the potentially detrimental effects of these boundaries, a wide aspect model ratio is necessary. Increasing the dimensions of the temperature model to three decreases convergence time by the nodal widths of the model in both the x and y directions, by 150 km and 110 km respectively for our model of northern England. To reduce computational intensity, therefore, we adopt a shallow lower boundary condition of 665.6 °C at 30 km depth, in concurrence with results from our one-dimensional lithosphere-scale model (Fig. 6), and assume the resolution of our model in terms of node spacing within the temperature grid is 500 m.

4.3 Approximation of geological model

The shortcomings of a finite difference model relate to its inflexibility. In implementing a finite difference methodology, the value for radiogenic heat production of a single node comprises heat production for the entire cubic rock volume for which that node represents. Likewise, for thermal conductivity, one value calculated between two adjacent nodes represents the combined conductivity for that transect of rock, which is 500 m long in this instance. Where the modelled rock volume is structurally complex or characteristically heterogeneous, therefore, thermal properties for individual temperature nodes may be misrepresentative, rendering the temperature model inaccurate. These issues are exacerbated when coarse model resolutions are necessary, as they are here. We thus demonstrate how more representative 3D thermal property matrices may be derived from structurally complex geological models.

Thermal properties for distinct points within the bounds of our 3D temperature model reflect the corresponding depths of those points at specific x and y coordinates relative to the depths of geological boundaries in a geological model. Depending on the preassigned distance between temperature nodes (∇i), the corresponding depth of a temperature node in a geological model is determined by:

$$depth = (z - 1)\,\nabla i$$

(Eq. 5)

Where z is a reference to the depth corresponding to the position of a given node within the temperature matrix.

Geological boundaries separate the numerous units of our geological model, which are assigned a series of distinct thermal properties (Table 1). So that we may avoid removing any of our geological model that is situated above sea level, the depths of geological horizons are given relative to surface elevation.

4.3.1 Thermal conductivity matrices

We overcome resolution issues for thermal conductivity tensors between adjacent temperature nodes, i.e. $k_{i+1/2}$ and $k_{i-1/2}$, by finding the harmonic mean (Hantschel and Kauerauf, 2009) of multiple thermal conductivity values at uniformly spaced points between the respective nodes. Depending on the interval spacing resolution (res) of sampled k points relative to temperature node spacing (∇i), the distance between these sampling points (ss) is determined as:

$$ss = {}^{\nabla i}/_{res}$$

(Eq. 6)

We adopt a resolution 50 times that of our temperature node spacing so that ss = 10 m.

For each node within our temperature matrix there are references to depths of geological boundaries at corresponding x and y coordinates of our geological model. The precision of these depth values is not fixed to the resolution of our temperature model. Therefore, determining thermal conductivity values for distinct points at x and y coordinates between vertically adjacent temperature nodes based on their corresponding depths within a geological model is uncomplicated. However, as inputted spatial data for geological boundaries are limited to the x and y coordinates of our temperature matrix, we may not apply this exact method to determine more representative thermal conductivity tensors laterally in between temperature nodes. To avoid inputting finer and more computationally intensive spatial data for geological boundaries, we interpolate depths of geological boundaries between laterally adjacent temperature nodes. These interpolated depths are used as a basis for determining k values in between laterally adjacent temperature nodes. The harmonic mean of these values may then be determined.

4.3.2 Radiogenic heat production matrices

Poor resolutions for Q value matrices are not as detrimental to the accuracy of predictive subsurface temperature models as k value matrices. Nonetheless, more representative matrices of Q values may be attained by adopting similar approaches to those just described for thermal conductivity. We determine Q values for multiple points up to half the temperature node spacing away from a given temperature node in the x, y and z directions, which is 250 m in this instance. We manage this by adopting the same technique for determining k values at points in between temperature nodes in the z direction, and the x and y directions respectively. The arithmetic mean of these values is then determined (Hantschel and Kauerauf, 2009).

Figure 7 illustrates the benefit of deriving more accurate thermal property matrices from geological models in this way. Compared with finding the harmonic mean between just two conductivity values at points corresponding to adjacent temperature nodes, our more accurate thermal conductivity matrix is smoother. Sharp lateral conductivity changes correspond only to steeply dipping beds or fault offsets in this more accurate scenario (Fig. 7a), rather than also shallowly dipping beds or the variable dips of beds with vertical thicknesses less than our temperature node spacing (Fig. 7b).

5. 3D temperature simulation

Our 3D subsurface temperature model reflects the controls of geological structure on vertical and lateral heat transfer and heat production. Temperatures calculated at depths of less than approximately 5 km are influenced by a combination of sedimentary basin fill and heat producing granite intrusions within the basement. At depths greater than 5 km, the basement has a predominant control on temperature distribution. We ignore parts of our model that are less than 10 km away from the lateral boundaries that are more strongly influenced by boundary conditions.

5.1 Predicted shallow subsurface temperatures

The dominant 'hot spots' at 1 km depth are situated upon the central part of the Alston Block (Fig. 2a), the northern part of the Solway Syncline, the southern part of the Bewcastle Anticline, along the Vale of Eden and along the eastern margins of the Alston Block, and the Stainmore Trough (Fig. 8a). The modelled hot spot at 1 km depth on the central part of the Alston Block, where temperatures reach 46 °C, correlates strongly with the North Pennine Batholith (Fig. 2b). However, the absence of any such hot spot in the Lake District, which is underpinned by the Lake District Batholith, at 1 km depth suggests that other factors influence this particular hot spot. We suggest that elevated temperatures on the Alston Block are influenced also by the local, variably thick, and comparatively insulating Carboniferous cover (*cf*. Bott *et al*., 1972) (Fig. 4). This cover thickens towards the east and incorporates progressively younger and more insulating coal-bearing strata. These trends may account for the preservation of greater heat at 1 km depth towards the vertically adjacent eastern margin of the heat producing North Pennine Batholith, despite the eastwards thinning of this structure here (Kimbell *et al*., 2010).

Owing to the comparatively thick and thermally insulating sedimentary fill preserved in the Vale of Eden Basin and lateral heat transfer from the radiothermal Lake District and North Pennine batholiths, our 3D subsurface temperature model predicts elevated temperatures at 1 km in this region, up to 43 °C (Fig. 8a). The parallel, NNE-SSW orientated Solway Syncline and Bewcastle Anticline provide more interesting thermal anomalies at 1 km depth. The northern part of the Solway Syncline, is comparatively hot at 1 km depth, up to 43 °C. Towards the south where this structure plunges, modelled temperatures at 1 km decrease to less than 39 °C. Conversely, the northern part of the Bewcastle Anticline is coolest, less than 37 °C, where thermally conductive pre-Carboniferous basement rock is shallowest. Where this structure also plunges to the south and preserves progressively thicker and younger insulating Carboniferous strata, temperatures increase up to 43 °C. Some of these thermal trends may be explained by the non-uniform presence and comparative thicknesses of coal-bearing and thermally insulating strata in this part of the Northumberland-Solway Basin. Some other thermal trends, however, may instead be explained by the vertical distributions of variably conductive rock units within the subsurface and the effects of these distributions on geothermal gradients at different depths. Transitioning from relatively insulating to conducting rock units with depth results in a decreased geothermal gradient with depth. The opposite arrangement results in an increased geothermal gradient with depth. Because the thermally insulating Pennine Coal Measures Group is at depths greater than 2 km to the south of the Solway Syncline, towards where the fold plunges, the geothermal gradient at these depths here is greater. Resulting temperatures at shallower depths, 1 km depth, are less. In contrast, in the northern part of the Solway Syncline, the thermally insulating Coal Measures are at depths between

0.5 and 2 km. As a result, the geothermal gradient is steepest at these depths and temperatures at 1 km are comparatively elevated.

5.2 Predicted deep subsurface temperatures

Maximum vertical sedimentary basin thickness in our study area is approximately 8 km. Around these depths, little is known about the characteristics of basin fill (*cf*. Chadwick *et al*., 1995) so differentiating thermal properties is difficult. The two main hot spots for these depths are associated with the radiothermal Lake District and North Pennine batholiths, where temperatures reach up to 154 °C (Fig. 8c). Faintly elevated temperatures at 5 km depth (Fig. 8b) are associated with the Solway Syncline and the eastwards thickening of Carboniferous strata within the northern Pennine Basin. At 7 km depth, elevated temperatures associated with the Solway Syncline are diminished further, as the modelled geotherm equilibrates laterally as it approaches the lower boundary condition (Fig. 8c). Slight local temperature elevations may be associated with the greater thicknesses of Carboniferous strata towards the east of our study area, up to 190 °C. At these depths, however, any other sources of localized temperature anomalies are dwarfed by comparison with anomalies due to the Lake District and North Pennine batholiths.

5.3 Predicted isotherm depth

By cubically interpolating vertically between temperature nodes, we determine depth to the 100 °C isotherm across our study area. Depth to this temperature boundary varies between approximately 2.87 km and 3.51 km below surface in our study area (Fig. 9). The modelled isotherm is shallowest in the Lake District, although boundary conditions may exaggerate these shallow depths. The isotherm is also shallower than 3 km in the Alston Block, in the centre of our study area and towards Newcastle-upon-Tyne, suggesting that the two radiothermal granite intrusions of our study area strongly influence these depths. Markedly shallower depths, between approximately 3 km and 3.2 km below surface, for the isotherm are also predicted for the Solway Basin, the Vale of Eden Basin and the eastern part of our study area. In these areas, comparatively thick Pennine Coal Measures Group successions are preserved. The greatest depths to the 100 °C isotherm are predicted in the western and central parts of the Northumberland Basin and in the Southern Uplands.

5.4 Predicted heat flow

We solve the heat flow equation (Eq. 1), using the modelled temperature difference (∇T) and vertical thermal conductivity (k) (e.g. Fig. 7) between temperature nodes at surface and 500 m below surface, to determine surface heat flow density (Fig. 10). Because the heat flow equation integrates thermal conductivity and temperature gradient, areas where predicted heat flow is comparatively elevated with respect to the remainder of our study area do not perfectly conform to subsurface temperature 'hot spots' (Fig. 8). Instead, areas with elevated surface heat flow density correspond to regions where shallow subsurface temperatures and bedrock conductivity are high, such as on the central and eastern parts of the Alston Block and the Lake District. In these areas, predicted surface heat flow exceeds 90 mW m^{-2}. Predicted heat flow in our case study area is more strictly aligned to depositional settings during early Carboniferous rifting (e.g. Howell *et al*., 2019) than subsurface temperature. Comparatively uplifted pre-Carboniferous basement blocks have overall greater heat flow whereas deeper basins, which were typically infilled by thermally insulating sedimentary rock, have overall lower heat flow.

6. Model verification

To demonstrate the accuracy of our subsurface temperature model, we compare our predictions against results from previous studies, including resource maps based on contouring methods (e.g. Fig. 1), and measured equilibrium borehole temperatures from our case study area. We also consider variations between results from our thermal model and temperature measurements that may not be resolved by adopting our predictive modelling technique.

6.1 Comparisons of modelled and measured subsurface temperature data

Overall, there is a wide dispersion of temperatures of temperatures at 1 km depth in our study area (Fig. 11a). Our mean modelled temperature at 1 km depth of 41.36 °C indicates an average shallow geothermal gradient of 31.36 °C km^{-1}, which is slightly greater than the UK average of 28 °C km^{-1}, although our study area is widely considered to be geothermally hotter than much of the rest of the UK (Busby *et al.*, 2011). There are broad similarities between the distributions of modelled hot and cold temperature anomalies (Fig. 8) and predicted anomalies based on contouring (Fig. 3).

Equilibrium borehole temperature measurements effectively remove drilling induced transient temperature effects (Oxburgh *et al.*, 1972). Analyzing these data, when possible, should be considered an integral part of verifying predictive temperature models. Our predicted subsurface temperatures show strong similarities with measured temperatures from the Rookhope Borehole (Fig. 11d), which are described in detail by Bott *et al*. (1972). In particular, the decreased geothermal gradient after approximately 450 m depth below surface is well reproduced by our modelling methodology. This depth corresponds to the top (Caledonian) basement unconformity, which locally separates overlying and comparatively thermally insulating Carboniferous sediments from the more conductive and radiogenic North Pennine Batholith.

There are stronger dissimilarities between our predicted subsurface temperatures and measured equilibrium temperatures from the Newcastle Science Central Deep Geothermal Borehole (Younger *et al.*, 2016) (Fig. 11e). The implementation of our modelling methodology under-predicts the temperature gradient with respect to measured temperatures in this region. This under-prediction could perceivably be attributed to the spatial variability of thermal properties (*cf*. Fuchs *et al*., 2020), or to the Ninety Fathom and Stublick fault system, which cuts across this region as well as geothermally hotter regions to the west (Fig. 2a). If these faults behave as non-sealing conduits, they may facilitate accelerated heat fluxes via fluid convection (*cf*. Calcagno *et al*., 2014).

The greatest disconnect between predicted and measured equilibrium temperature is associated with the youngest and most scarcely preserved Carboniferous sediments of our study area that are encountered in the Becklees borehole (*cf*. Jones *et al*., 2011) (Fig. 11f). Like temperatures in the Becklees borehole, our predicted geothermal gradient steepens between 500 and 1000 m depth below surface. For predicted subsurface temperatures, this is due to the presence of thermally insulating Pennine Coal Measures Group stratigraphy within our geological model between these depths (Chadwick *et al*., 1995) (Fig. 4). Instead of encountering a thick succession solely of this insulating rock unit, however, the Becklees borehole encounters approximately 600 m of sandstone-rich and variably porous sedimentary rock belonging to the Warwickshire Group, overlaying an approximately 500 m thick succession of the Pennine Coal Measures Group (Jones *et al*., 2011) (Fig. 12). These overlaying units are likely to be more conductive due to their compositions (e.g. Rybach, 1981) and may provide high permeability pathways for heat convection. Modelled subsurface temperatures may be over-predicted with respect to measured temperatures in the Becklees borehole as a result (Fig. 11f). However, as most of the remainder of Carboniferous sediments in northern England are typically tight (e.g. Younger *et al*., 2016), we choose to acknowledge these sources of inaccuracy and maintain our simplistic, yet more robust, modelling approach.

6.2 Comparisons of modelled and measured heat flow density data

Contoured heat flow density maps provide more precise constraints for our temperature model, given the greater density of heat flow data in our case study area (Fig. 1b). The two bullseyes over the Lake District and Alston Block, where heat flow is locally greater than 90 mW m^{-2}, are broadly replicated, as are the lower heat flows in the Northumberland-Solway Basin and Stainmore Trough (Fig. 10). Our temperature simulations offer greater resolution compared with these contoured resource maps. Figure 11d shows a cross-plot for measured heat flow data and modelled data taken from equivalent locations. Overall, there is a positive correlation, suggesting that our modelling technique successfully replicates areas of greater heat flow density. However, the dispersion of modelled heat flow density data falls short of equivalent measured data (also see Fig. 11b). This is indicated by the shallow cross-plot gradient of 0.2 (Fig. 11b).

At these shallow (<500 m) depths, modelled heat flow inaccuracies could perceivably be attributed to the neglected influences of superficial deposits, given that in northern England, many heat flow measurements were recorded in the shallowest tens of metres of the subsurface (Burley *et al*., 1984), and that superficial cover thicknesses locally exceed 60 m (McMillan, 2011). Whilst neglecting the influences of superficial cover has not had a noticeably detrimental effect on subsurface temperature predictions (e.g. Figs. 8, 11d, e and f), their admission appears to have more negatively impacted the dispersion of surface heat flow density data (Fig. 11c), because these data are more directly proportional to the thermal conductivity of the shallow subsurface (Eq. 1). In temperate regions of the world, including northern England, transient temperature effects relating to palaeoclimate are proven to also have detrimental effects on shallow heat flow density predictions (e.g. Slagstad *et al*., 2009; Majorowicz *et al*., 2012). A steady-state subsurface temperature model is, by definition, incapable of accounting for these effects; although a simplistic alternation to the temperature model's top boundary condition following temperature convergence, and repeated model iterations, would effectively replicate this transient effect. A surface heat flow over-estimation would be anticipated had the effects of transient climate adjustment had a detrimental effect on modelled heat flow data (Majorowicz *et al*., 2012). Nonetheless, a comparison between modelled and measured heat flow density data suggests no consistent over-estimation (Fig. 11e).

7. Discussion and conclusions

Predictive subsurface temperature and heat flow density maps can be extracted from our finite difference models (Figs. 8, 9 and 10) that are more resolute and geologically realistic compared to maps constructed by contouring around sparsely distributed and often unreliable data points (Fig. 1). Due to our averaging technique, the resolution of our geological model is scarcely compromised to reduce computational intensity. Its main strengths are its robustness, simplicity, and reproducibility relative to more elaborate finite element techniques (e.g. Cacace and Jacquey, 2017). Compared to other finite difference techniques (e.g. Fullea *et al*., 2009; Keller *et al*., 2020), our methodology offers more resolute, geologically more realistic, and quicker solutions for regional scale (>10 km) problems such subsurface temperature and heat flow density mapping. The main inaccuracies of our model in northern England relate to geological inputs, such as bedrock and superficial cover. Fuchs and Balling (2016) and Fuchs *et al*. (2020) discuss the importance of geological constraints and their regional variability for subsurface temperature models such as these. Other inaccuracies may relate to fluid convection. When deemed necessary and where data constraints are sufficient, the incorporation of fluid convection through rock units within temperature calculations may comprise a simple upgrade on these methods. However, to predict the influences of more complex structures, such as permeable fault zones, on subsurface temperature, more elaborate methods and finer resolution models may be necessary (*cf*. Calcagno *et al*., 2014). The method presented here represents a useful tool for understanding controls on subsurface temperature distribution and geothermal potential. MATLAB scripts and program files for our northern England temperature model are included within the supplementary information.

Acknowledgements

This manuscript contains work conducted during a PhD study undertaken as part of the Natural Environment Research Council (NERC) Centre for Doctoral Training (CDT) in Oil & Gas [grant number: NEM00578X/1]. It is sponsored by Natural Environment Research Council, the Keele University Acorn Fund and the National Productivity Investment Fund (NPIF) whose support is gratefully acknowledged.

Our 3D geological model was manipulated using Petrel (Schlumberger) software. Our temperature modelling technique is supported by the MATLAB (Mathworks) numerical computing environment.

Conflict of interest

The authors declare no conflict of interest.

Computer code availability

Name of code: Geothermal-Modelling

Developer: Louis Howell (l.p.howell@keele.ac.uk)

Year first available: 2020.

Hardware required: Our temperature modelling technique is supported by the MATLAB (Mathworks) numerical computing environment.

Program language: MATLAB.

Program size: 30 MB (including geological model).

Source code: https://github.com/lphowell/Geothermal-Modelling

References

Adams, C., Monaghan, A. and Gluyas, J., 2019. Mining for heat. *Geoscientist*, *29*(4), pp.10-15. http://nora.nerc.ac.uk/id/eprint/523186/

Bayer, U., Scheck, M. and Köhler, M., 1997. Modeling of the 3D thermal field in the northeast German basin. *Geologische Rundschau*, *86*(2), pp.241-251. https://doi.org/10.1007/s005310050137

Bott, M.H.P., Johnson, G.A.L., Mansfield, J. and Wheilden, J., 1972. Terrestrial heat flow in north-east England. *Geophysical Journal International*, *27*(3), pp.277-288. https://doi.org/10.1111/j.1365-246X.1972.tb06093.x

BP, 2019. BP Energy Outlook 2019 edition. *London, United Kingdom*.

British Geological Survey, 2008. *Digital Geological Map of Great Britain 1:625 000 scale (DiGMapGB-625), Bedrock data. Version 5.17*. Keyworth, Nottingham: British Geological Survey. Release date 11-2-2008.

Burley, A.J., Edmunds, W.M. and Gale, I.N., 1984. Investigation of the geothermal potential of the UK: catalogue of geothermal data for the land area of the United Kingdom. http://nora.nerc.ac.uk/id/eprint/512272/

Busby, J., Lewis, M., Reeves, H. and Lawley, R., 2009. Initial geological considerations before installing ground source heat pump systems. *Quarterly Journal of Engineering Geology and Hydrogeology*, *42*(3), pp.295-306. https://doi.org/10.1144/1470-9236/08-092

Busby, J., 2010. Geothermal prospects in the United Kingdom. In: *Proceedings World Geothermal Congress 2010*, Bali, Indonesia, 25-29 April. http://nora.nerc.ac.uk/id/eprint/15965/1/GeothermalProspectsUK.pdf

Busby, J., Kingdon, A. and Williams, J., 2011. The measured shallow temperature field in Britain. *Quarterly Journal of Engineering Geology and Hydrogeology*, *44*(3), pp.373-387. https://doi.org/10.1144/1470-9236/10-049

Busby, J., 2014. Geothermal energy in sedimentary basins in the UK. *Hydrogeology journal*, *22*(1), pp.129-141. https://doi.org/10.1007/s10040-013-1054-4

Busby, L.P., 2019. Thermal conductivity and subsurface temperature data pertaining to the Glasgow Geothermal Energy Research Field Site (GGERFS). *British Geological Survey Open Report*, OR/19/015. 21pp. http://nora.nerc.ac.uk/id/eprint/523450/1/OR19015.pdf

Cacace, M., Kaiser, B.O., Lewerenz, B. and Scheck-Wenderoth, M., 2010. Geothermal energy in sedimentary basins: What we can learn from regional numerical models. *Geochemistry*, *70*, pp.33-46. https://doi.org/10.1016/j.chemer.2010.05.017

Cacace, M. and Jacquey, A.B., 2017. Flexible parallel implicit modelling of coupled thermal–hydraulic–mechanical processes in fractured rocks. *Solid Earth*, *8*, pp.921-941. https://doi.org/10.5194/se-8-921-2017

Calcagno, P., Baujard, C., Guillou-Frottier, L., Dagallier, A. and Genter, A., 2014. Estimation of the deep geothermal potential within the Tertiary Limagne basin (French Massif Central): An integrated 3D geological and thermal approach. *Geothermics*, *51*, pp.496-508. https://doi.org/10.1016/j.geothermics.2014.02.002

Čermác, V. and Rybach, L., 1982. Thermal properties: Thermal conductivity and specific heat of minerals and rocks. *Landolt-Börnstein Zahlenwerte und Functionen aus Naturwissenschaften und Technik, Neue Serie, Physikalische Eigenschaften der Gesteine*, pp.305-343.

Chadwick, B.A., Holliday, D.W., Holloway, S., Hulbert, A.G. and Lawrence, D.J.D., 1995. The structure and evolution of the Northumberland-Solway Basin and adjacent areas. Subsurface memoir of the British Geological Survey. London: HMSO.

Croucher, A., O'Sullivan, M., O'Sullivan, J., Yeh, A., Burnell, J. and Kissling, W., 2020. Waiwera: A parallel open-source geothermal flow simulator. *Computers & Geosciences*, p.104529. https://doi.org/10.1016/j.cageo.2020.104529

Downing, R.A. and Gray, D.A., 1986a. Geothermal resources of the United Kingdom. *Journal of the Geological Society*, *143*(3), pp.499-507. https://doi.org/10.1144/gsjgs.143.3.0499

Downing, R.A. and Gray, D.A., (eds.) 1986b. Geothermal Energy—the Potential in the United Kingdom. HMSO, London

Fuchs, S. and Balling, N., 2016. Improving the temperature predictions of subsurface thermal models by using high-quality input data. Part 1: Uncertainty analysis of the thermal-conductivity parameterization. *Geothermics*, *64*, pp.42-54. https://doi.org/10.1016/j.geothermics.2016.04.010

Fuchs, S., Balling, N. and Mathiesen, A., 2020. Deep basin temperature and heat-flow field in Denmark–New insights from borehole analysis and 3D geothermal modelling. *Geothermics*, *83*, p.101722. https://doi.org/10.1016/j.geothermics.2019.101722

Fullea, J., Afonso, J.C., Connolly, J.A.D., Fernandez, M., García-Castellanos, D. and Zeyen, H., 2009. LitMod3D: An interactive 3-D software to model the thermal, compositional, density, seismological, and rheological structure of the lithosphere and sublithospheric upper mantle. *Geochemistry, Geophysics, Geosystems*, 10(8). https://doi.org/10.1029/2009GC002391

Gibson, H., Stüwe, K., Seikel, R., FitzGerald, D., Calcagno, P., Guillen, A., and McInerney, P., 2008. Forward prediction temperature distribution direct from 3D geology models. In: *Proceedings of the Australian Geothermal Energy Conference*, Melbourne 2008.

Hantschel, T. and Kauerauf, A.I., 2009. Introduction to Basin modeling. In: *Fundamentals of Basin and Petroleum Systems Modeling* (pp. 1-30). Springer, Berlin, Heidelberg.

Hirst C.M., 2012. The geothermal potential of low enthalpy deep sedimentary basins in the UK. PhD Thesis, Durham University, UK.

Howell, L., Egan, S., Leslie, G. and Clarke, S., 2019. Structural and geodynamic modelling of the influence of granite bodies during lithospheric extension: application to the Carboniferous basins of northern England. *Tectonophysics*, *755*, pp.47-63. https://doi.org/10.1016/j.tecto.2019.02.008

Howell, L.P., Besly, B.M., Sooriyathasan, S., Egan, S.S. and Leslie, A.G., *in press*. Seismic and borehole-based mapping of the late Carboniferous succession in the Canonbie Coalfield, SW Scotland: evidence for a 'broken' Variscan foreland? *Scottish Journal of Geology*.

Jones, N.S., Holliday, D.W. and McKervey, J.A., 2011. Warwickshire Group (Pennsylvanian) red-beds of the Canonbie Coalfield, England–Scotland border, and their regional palaeogeographical implications. *Geological Magazine*, *148*(1), pp.50-77. https://doi.org/10.1017/S001675681000035X

Kimbell, G.S., Young, B., Millward, D. and Crowley, Q.G., 2010. The North Pennine batholith (Weardale Granite) of northern England: new data on its age and form. *Proceedings of the Yorkshire Geological Society*, *58*(2), pp.107-128. https://doi.org/10.1144/pygs.58.1.273

Kimbell, G.S., Williamson, J.P., 2015. A gravity interpretation of the Central North Sea. *British Geological Survey Commissioned Report*, CR/15/119. 75pp. http://nora.nerc.ac.uk/id/eprint/516759/1/CR15119.pdf

Lee, M.K., Brown, G.C., Webb, P.C., Wheildon, J. and Rollin, K.E., 1987. Heat flow, heat production and thermo-tectonic setting in mainland UK. *Journal of the Geological Society*, *144*(1), pp.35-42. https://doi.org/10.1144/gsjgs.144.1.0035

Majorowicz, J., Gosnold, W., Gray, A., Safanda, J., Klenner, R. and Unsworth, M., 2012. Implications of post-glacial warming for northern Alberta heat flow-correcting for the underestimate of the geothermal potential. *GRC Transactions*, *36*(GRC1030303).

Manning, D.A.C., Younger, P.L., Smith, F.W., Jones, J.M., Dufton, D.J. and Diskin, S., 2007. A deep geothermal exploration well at Eastgate, Weardale, UK: a novel exploration concept for low-enthalpy resources. *Journal of the Geological Society*, *164*(2), pp.371-382. https://doi.org/10.1144/0016-76492006-015

McMillan, A.A., Hamblin, R.J.O., Merritt, J.W., 2011. A lithostratigraphical framework for onshore Quaternary and Neogene (Tertiary) superficial deposits of Great Britain and the Isle of Man. *British Geological Survey Research Report*, RR/10/03. 343pp. http://nora.nerc.ac.uk/id/eprint/14531/1/RR10003.pdf

Monaghan, A., Starcher, V., Barron, H., Kuras, O., Abesser, C., Midgley, J., Dochartaigh, B.Ó., Fordyce, F., Burke, S., Taylor-Curran, H. and Luckett, R., 2019. A new Mine Water Geothermal Research Facility: the UK Geoenergy Observatory in Glasgow, Scotland. In *81st EAGE Conference and Exhibition 2019* (Vol. 2019, No. 1, pp. 1-5). European Association of Geoscientists & Engineers. https://doi.org/10.3997/2214-4609.201901602

Norden, B. and Forster, A., 2006. Thermal conductivity and radiogenic heat production of sedimentary and magmatic rocks in the Northeast German Basin. *AAPG bulletin*, *90*(6), pp.939-962. https://doi.org/10.1306/01250605100

Norden, B., Förster, A. and Balling, N., 2008. Heat flow and lithospheric thermal regime in the Northeast German Basin. *Tectonophysics*, *460*(1-4), pp.215-229. https://doi.org/10.1016/j.tecto.2008.08.022

Norden, B., Förster, A., Förster, H.J. and Fuchs, S., 2020. Temperature and pressure corrections applied to rock thermal conductivity: impact on subsurface temperature prognosis and heat-flow determination in geothermal exploration. *Geothermal Energy*, *8*(1), pp.1-19. https://doi.org/10.1186/s40517-020-0157-0

Oxburgh, E.R., Richardson, S.W., Turcotte, D.L. and Hsui, A., 1972. Equilibrium bore hole temperatures from observation of thermal transients during drilling. *Earth and Planetary Science Letters*, *14*(1), pp.47-49. https://doi.org/10.1016/0012-821X(72)90077-5

Paulillo, A., Cotton, L., Law, R., Striolo, A. and Lettieri, P., 2020. Geothermal energy in the UK: the life-cycle environmental impacts of electricity production from the United Downs Deep Geothermal Power project. *Journal of Cleaner Production*, *249*, p.119410. https://doi.org/10.1016/j.jclepro.2019.119410

Pérez-Zárate, D., Santoyo, E., Acevedo-Anicasio, A., Díaz-González, L. and García-López, C., 2019. Evaluation of artificial neural networks for the prediction of deep reservoir temperatures using the gas-phase composition of geothermal fluids. *Computers & Geosciences*, *129*, pp.49-68. https://doi.org/10.1016/j.cageo.2019.05.004

Rollin, K.E., 1995. A simple heat-flow quality function and appraisal of heat-flow measurements and heat-flow estimates from the UK Geothermal Catalogue. *Tectonophysics*, *244*(1-3), pp.185-196. https://doi.org/10.1016/0040-1951(94)00227-Z

Rybach, L. 1981. Geothermal systems, conductive heat flow, geothermal anomalies. *In*: Rybach, L. and Muffler, L.J.P. (eds.), *Geothermal Systems: Principles and Case Histories*. Wiley, Chichester, 3-36.

Sclater, J.G. and Christie, P.A., 1980. Continental stretching: An explanation of the post-mid-Cretaceous subsidence of the central North Sea basin. *Journal of Geophysical Research: Solid Earth*, *85*(B7), pp.3711-3739. https://doi.org/10.1029/JB085iB07p03711

Slagstad, T., Balling, N., Elvebakk, H., Midttømme, K., Olesen, O., Olsen, L. and Pascal, C., 2009. Heat-flow measurements in Late Palaeoproterozoic to Permian geological provinces in south and central Norway and a new heat-flow map of Fennoscandia and the Norwegian–Greenland Sea. *Tectonophysics*, *473*(3-4), pp.341-361. https://doi.org/10.1016/j.tecto.2009.03.007

Terrington, R.L. and Thorpe, S., 2014. Metadata report for the Northumberland and Solway Basin 1:250 000 geological model. British Geological Survey Open Report, OR/13/049. 20pp. http://nora.nerc.ac.uk/id/eprint/507069/1/OR13049.pdf

Vilà, M., Fernández, M. and Jiménez-Munt, I., 2010. Radiogenic heat production variability of some common lithological groups and its significance to lithospheric thermal modeling. *Tectonophysics*, 490(3-4), pp.152-164. https://doi.org/10.1016/j.tecto.2010.05.003

Younger, P.L., Manning, D.A., Millward, D., Busby, J.P., Jones, C.R. and Gluyas, J.G., 2016. Geothermal exploration in the Fell Sandstone Formation (Mississippian) beneath the city centre of Newcastle upon Tyne, UK: the Newcastle Science Central deep geothermal borehole. *Quarterly Journal of Engineering Geology and Hydrogeology*, *49*(4), pp.350-363. https://doi.org/10.1144/qjegh2016-053

Zhang, X., Lyu, D., Li, P., Jin, X., Liaw, P.K. and Keer, L.M., 2019. A closed-form solution for the horizontally aligned thermal-porous spheroidal inclusion in a half-space and its applications in geothermal reservoirs. *Computers & Geosciences*, *122*, pp.15-24. https://doi.org/10.1016/j.cageo.2018.10.001

Figures

Figure 1

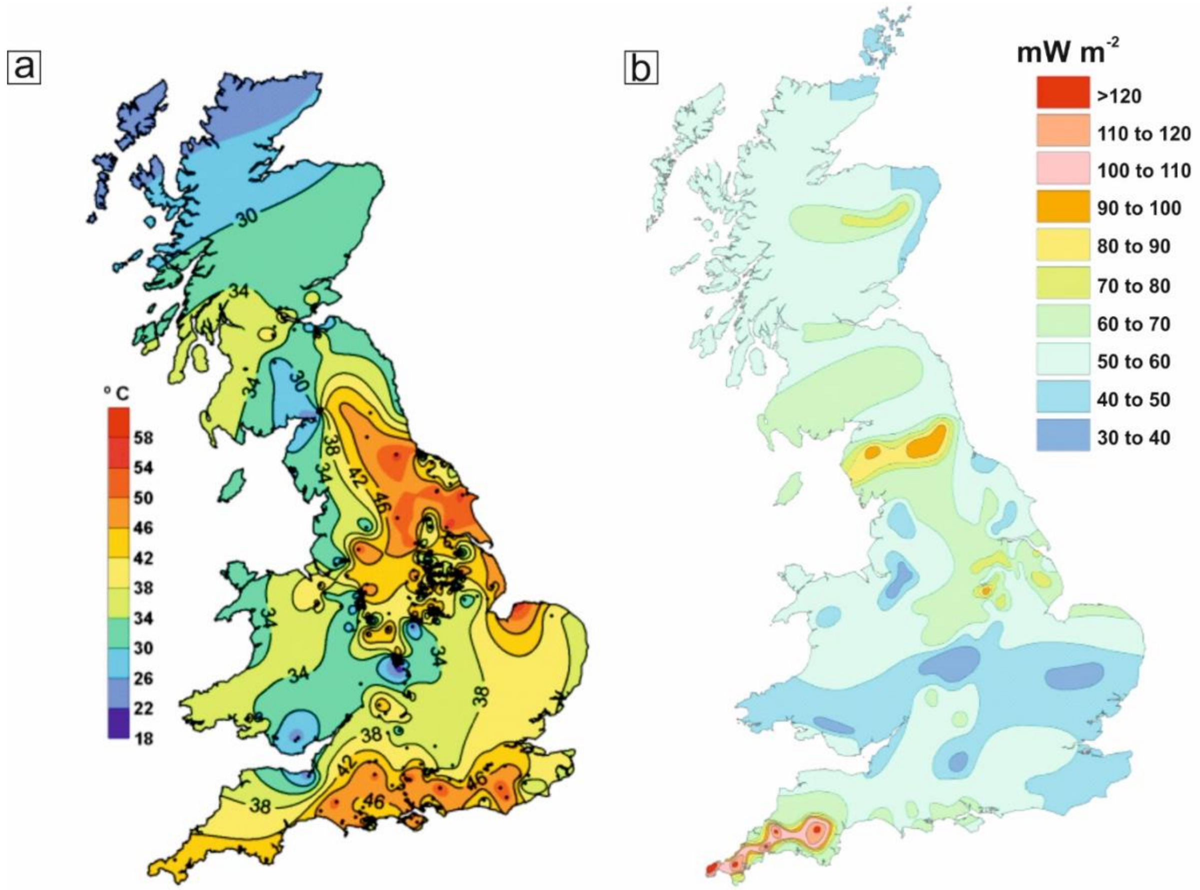

Fig. 1a: UK subsurface temperature maps for 1 km depth (after Busby *et al*., 2011). 1b: UK heat flow maps (after Downing and Gray, 1986).

Figure 2

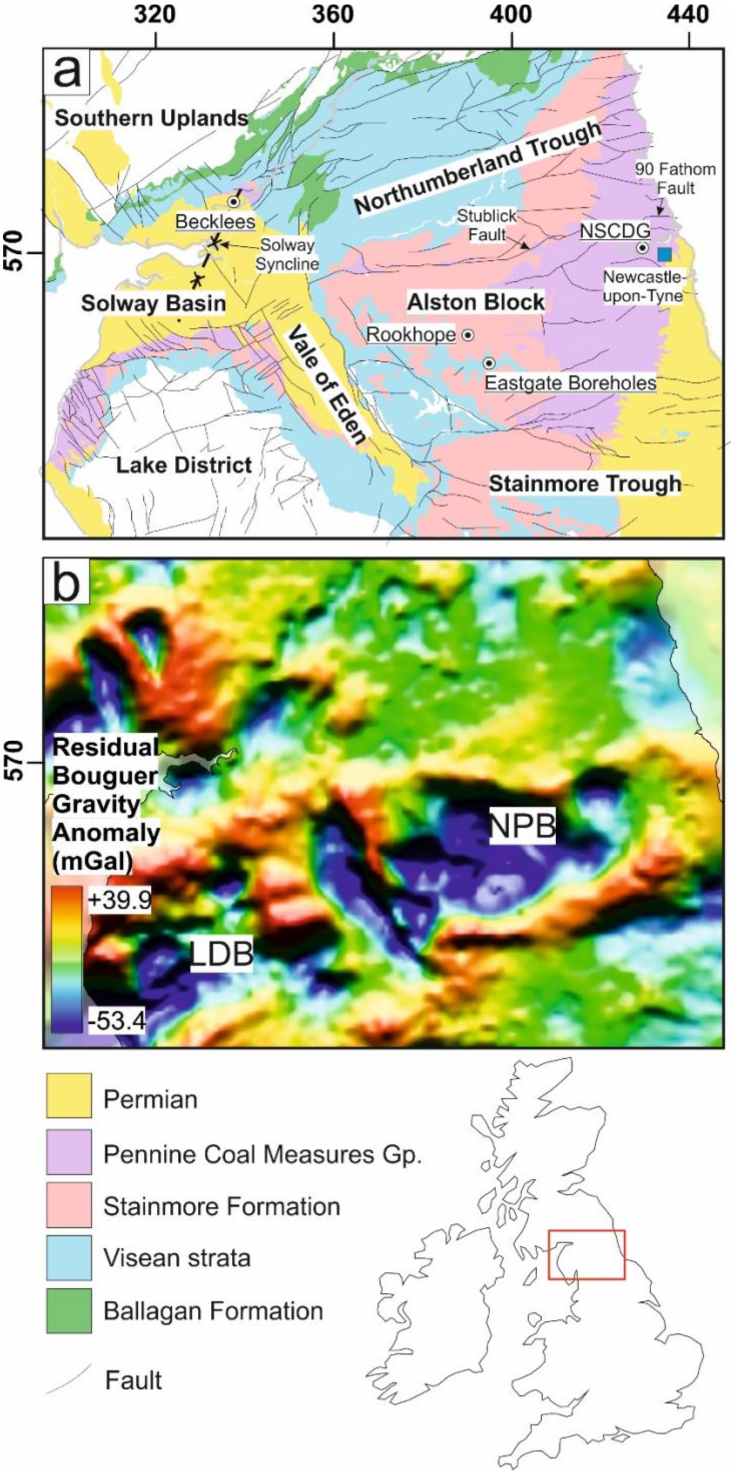

Fig. 2a: A geological map for our case study area (British Geological Survey, 2008) with annotated structural features and borehole locations. 2b: A Bouguer gravity anomaly survey for our case study area (Kimbell and Williamson, 2015) with annotations for the negative gravitational anomalies associated with the Lake District Batholith (LDB) and the North Pennine Batholith (NPB). British National Grid coordinates are used for these and all maps in this manuscript.

Figure 3

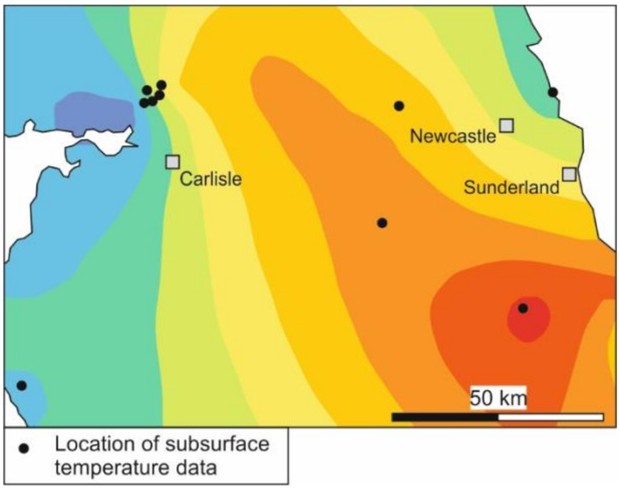

Fig. 3: Subsurface temperature contours (Fig. 1a) and locations of data points (*cf*. Burley *et al*., 1984).

Figure 4

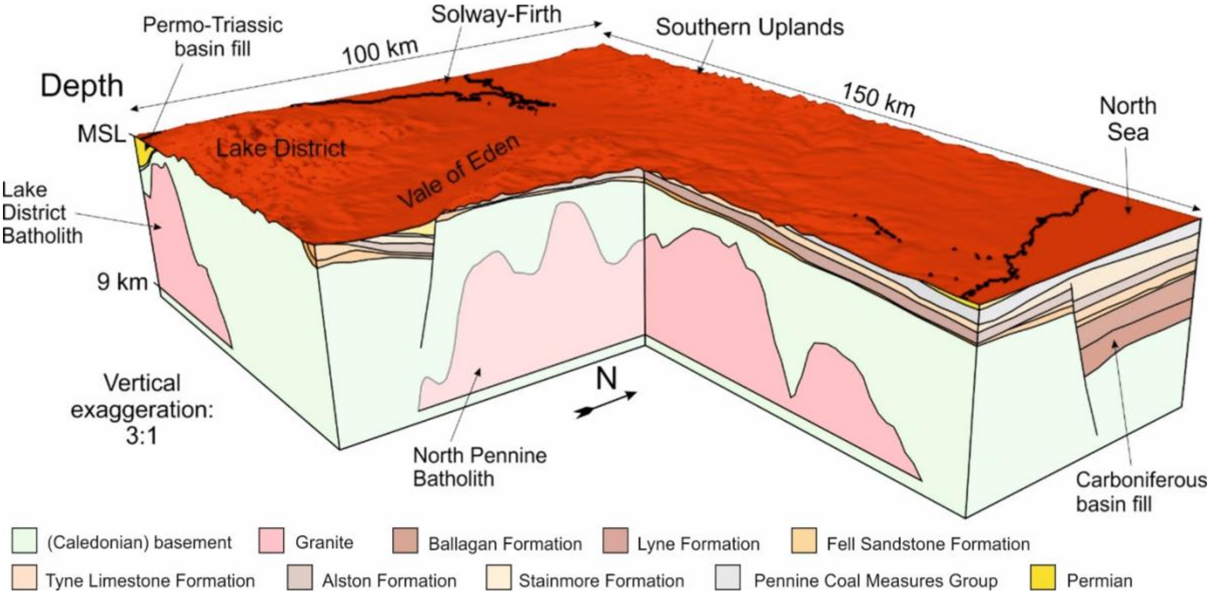

Fig. 4: A schematic illustration of our 3D geological model. Carboniferous basin structure after Chadwick *et al*. (1995) and Caledonian granite thicknesses after Kimbell *et al*. (2010). MSL = mean sea level. The depicted 3D model was produced using Petrel (Schlumberger) software.

Figure 5

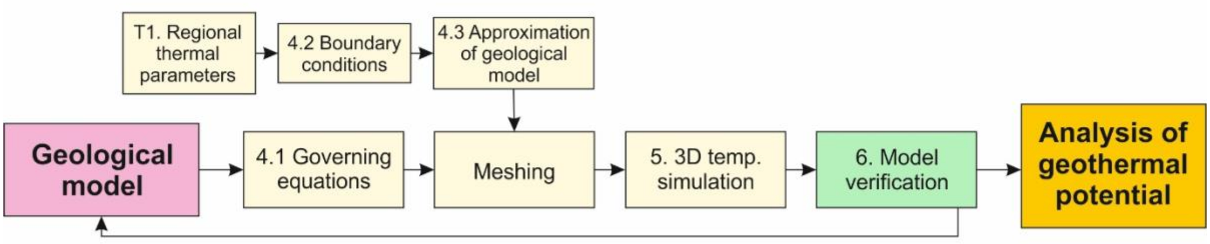

Fig. 5: An illustrated summary of our modelling approach. Numbering of method steps correspond to sections or tables within this manuscript, in which these steps are described.

Figure 6

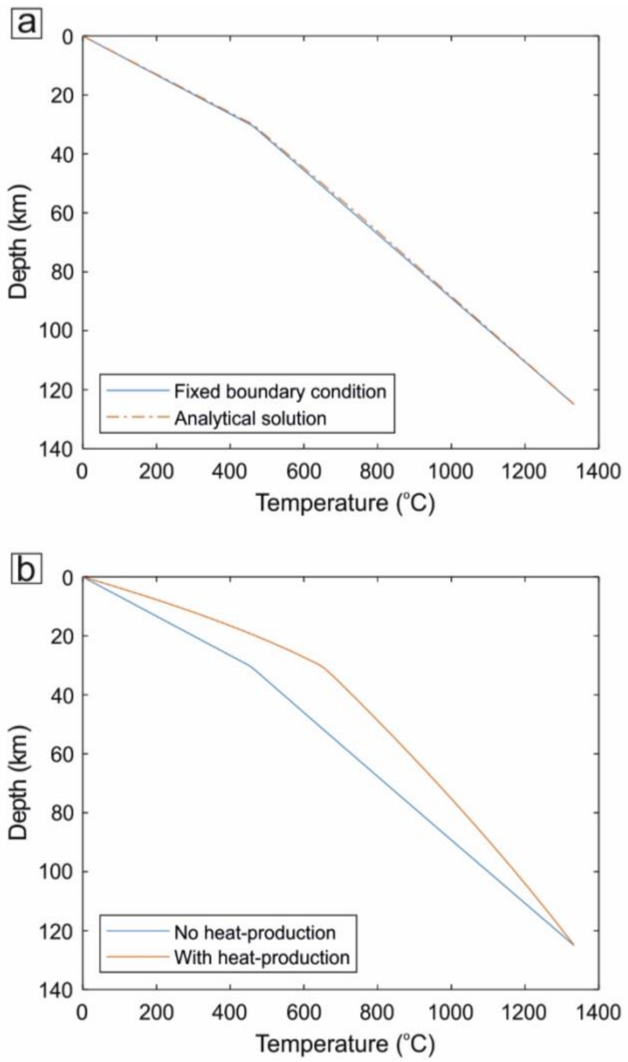

Fig. 6a: A comparison between analytical and fixed boundary condition solutions for one-dimensional lithosphere-scale non-homogeneous conductive heat flow. See Table 1 for modelling parameters. 6b: A comparison between fixed boundary condition solutions for one-dimensional lithosphere-scale non-homogeneous conductive heat flow with no internal heat production (Q) and with internal heat production.

Figure 7

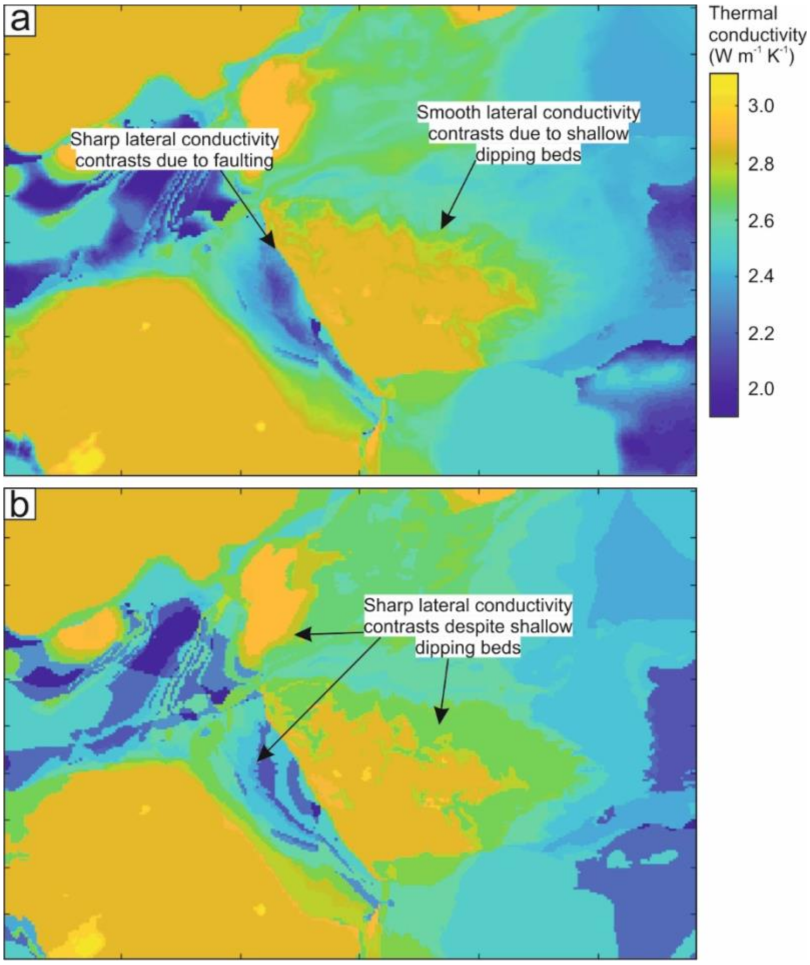

Fig. 7a: Vertical thermal conductivity tensors between 500 m and 1000 m below surface determined by calculating the harmonic mean of multiple values between these two depths for northern England. 7b: Vertical thermal conductivity tensors between 500 m and 1000 m below surface determined by calculating the harmonic mean of just the two values at temperature nodes. For thermal conductivity values of rock units see Table 1.

Figure 8

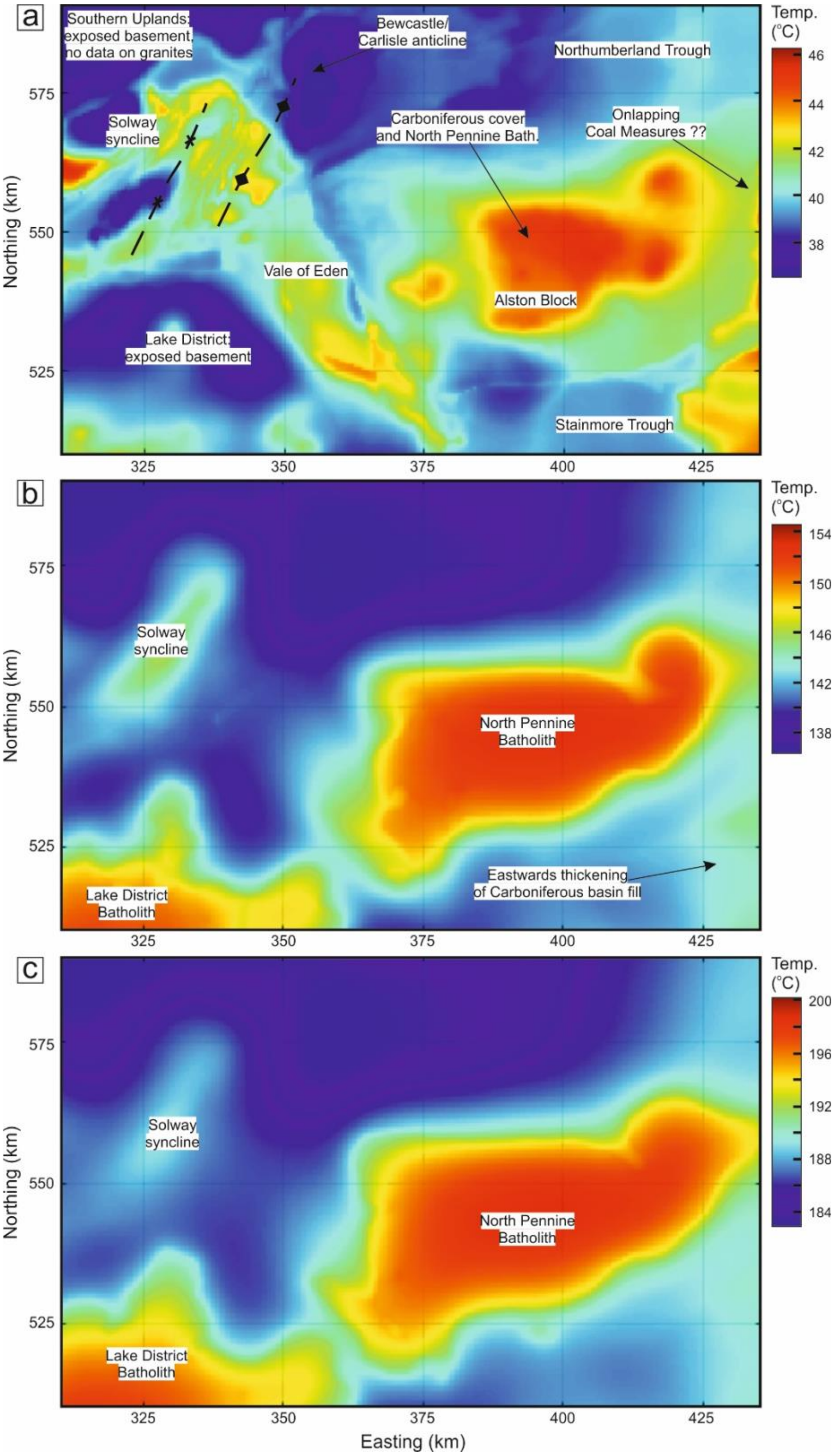

Fig. 8a: Modelled temperature at 1 km depth. Compare with Fig. 1b (Busby *et al*., 2011). 8b: Modelled temperature at 5 km depth. 8c: Modelled temperature at 7 km depth.

Figure 9

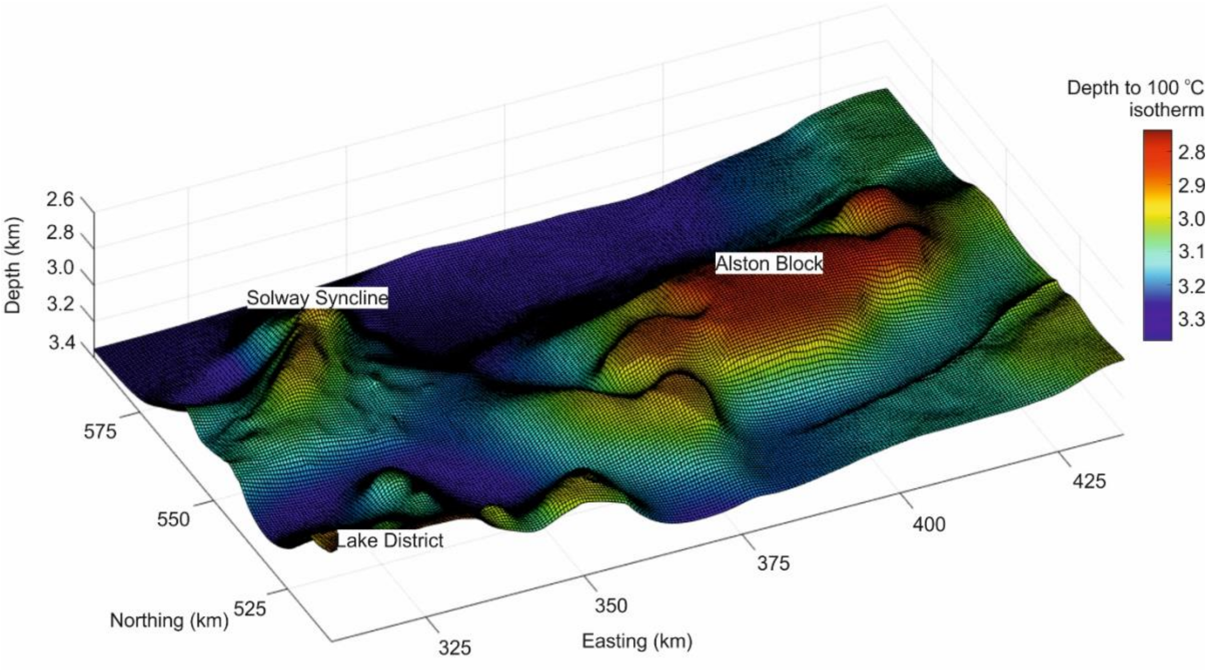

Fig. 9: Modelled depth to the 100 °C isotherm.

Figure 10

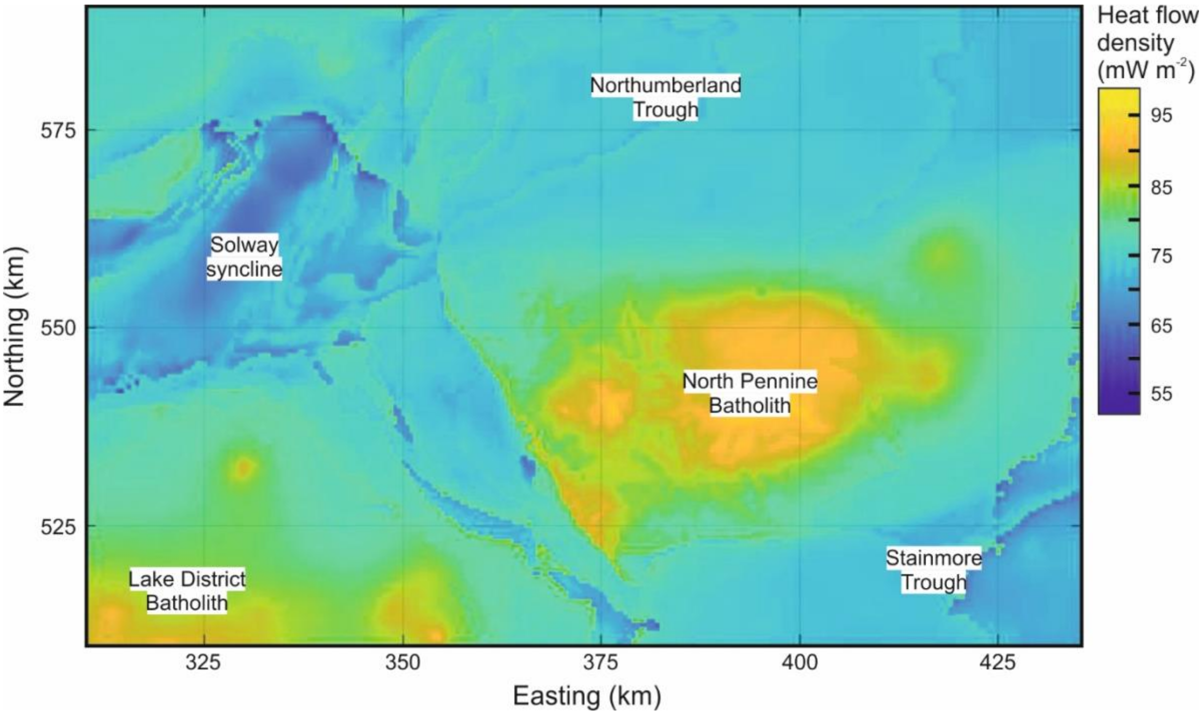

Fig. 10: Modelled surface (500 m below surface to surface) heat flow density map for northern England based on predicted subsurface temperatures and vertical conductivity values. Compare with Fig. 1b (Downing and Gray, 1986a).

Figure 11

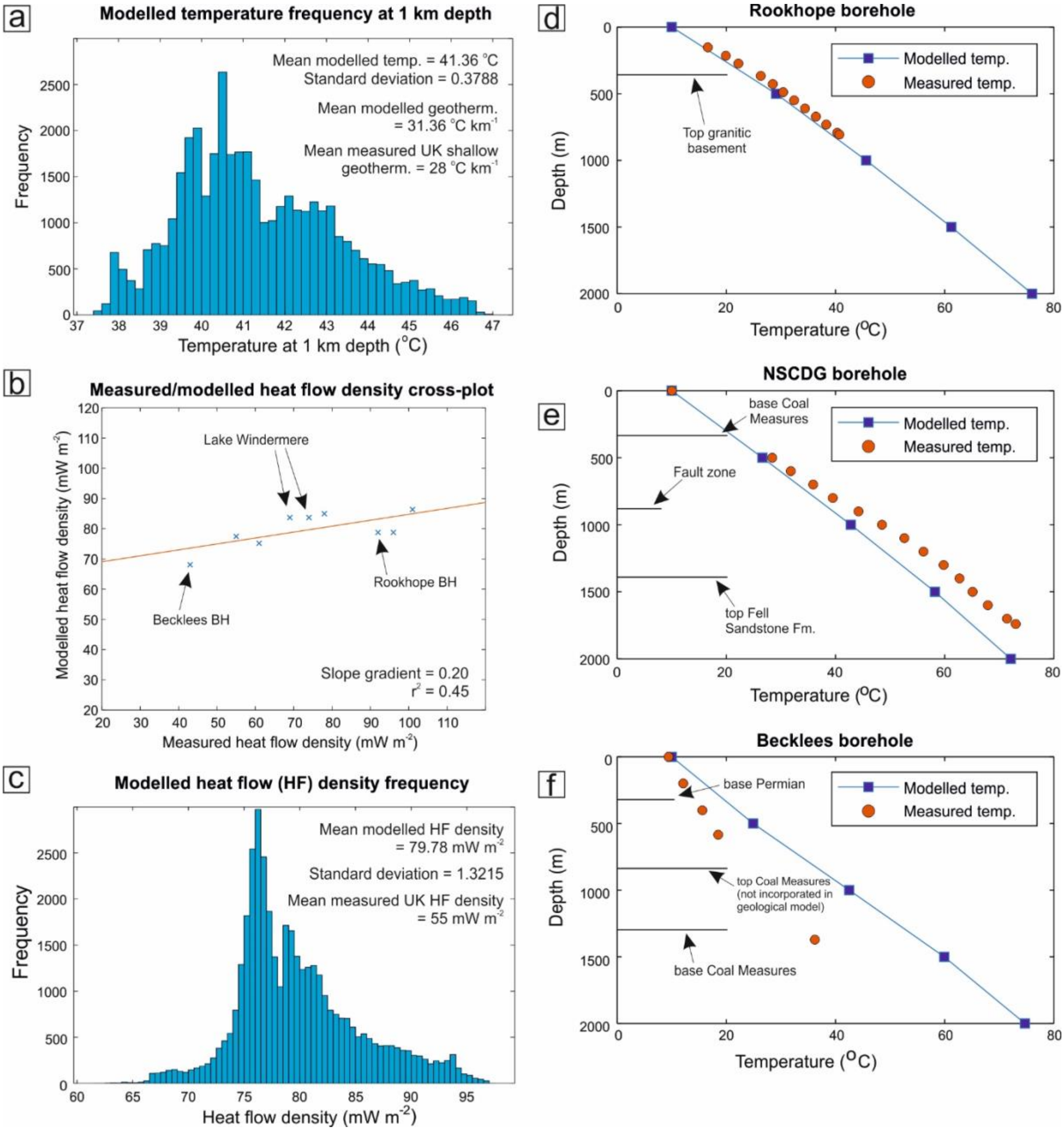

Fig. 11a: A cross-plot between measured heat flow density data and modelled data in our study area. Modelled data are taken from approximately the equivalent location as measured data. 11b and c: Frequency charts for modelled temperature values at 1 km depth, and shallow (<500 m) heat flow density values, respectively. Mean measured UK shallow (<1 km) geothermal gradient and mean measured UK heat flow density taken from Busby *et al*. (2011) and Busby (2010). 11d, e and f: Comparisons between modelled subsurface temperatures and measured equilibrium borehole temperatures for the Rookhope Borehole, the Newcastle Science Central Deep Geothermal Borehole and the Becklees Borehole, respectively. For locations of boreholes, see Figure 3a. Measured equilibrium boreholes temperatures taken from Burley *et al*. (1984) and Younger *et al*. (2016).

Figure 12

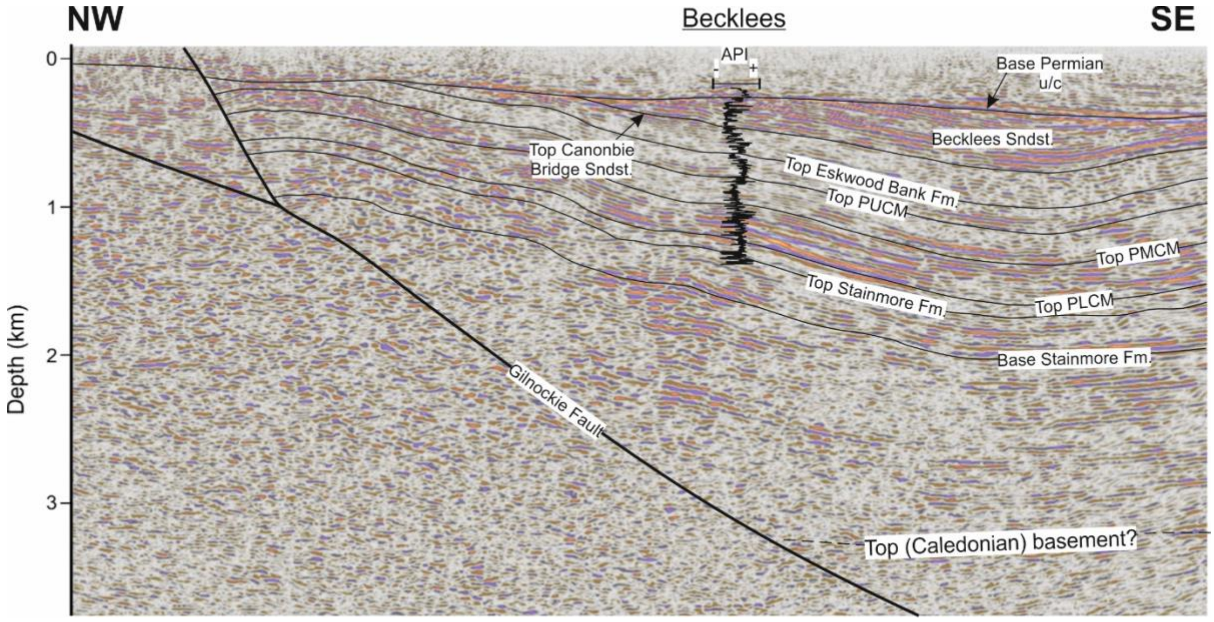

Fig. 12: A seismic reflection profile intersecting the Becklees borehole. A vertical gamma ray profile for the Becklees borehole is illustrated. The Warwickshire Group comprises the Eskbank Wood, Canonbie Bridge Sandstone and Becklees Sandstone formations (*cf*. Jones *et al*., 2011). The Pennine Coal Measures Group comprises the Pennine Lower Coal Measures (PLCM), Pennine Middle Coal Measures (PMCM) and Pennine Upper Coal Measures (PUCM) formations. Seismic interpretation based on Howell *et al*. (in press). Seismic courtesy of the UK Onshore Geophysical Library (UKOGL).

Tables

Geological unit	Thermal conductivity ($W\ m^{-1}\ K^{-1}$)	RHP ($\mu W\ m^{-3}$)	Reference
Lower Permian	2.5	1.0	Norden and Förster (2006)
Pennine Coal Measures Group	1.9	0.92	Downing and Gray (1986)
Stainmore Formation	2.38	0.88	Younger *et al*. (2016)
Alston Formation	2.5	0.88	Younger *et al*. (2016)
Tyne Limestone Formation	2.7	0.85	Younger *et al*. (2016)
Fell Sandstone Formation	2.6	0.85	Younger *et al*. (2016)
Lyne Formation	2.7	0.85	Younger *et al*. (2016)
Ballagan Formation	2.92	0.85	Downing and Gray (1986b)
Pre-Carboniferous (Caledonian) basement	2.87	1.49	Downing and Gray (1986b)
Granite Batholiths	3.1	4.1	Downing and Gray (1986b); Manning *et al*. (2007)
Middle-Lower crust	3.1-2.2	1.5	Norden and Förster (2006); Norden *et al*. (2008)
Mantle	4.1	0.1	Čermác and Rybach (1982); Vila *et al*. (2010)

Table 1: Regional thermal parameters for temperature simulation.

Supplementary information

MATLAB project files (https://github.com/lphowell/Geothermal-Modelling/tree/master/Geothermal_NEngland).